
Article:
Botha, JA, Hunter, TN orcid.org/0000-0003-3922-491X, Johannsmann, D et al. (6 more authors) (2019) Resonance properties of quartz crystal microbalance immersed in high solid content suspensions. Colloids and Surfaces A: Physicochemical and Engineering Aspects, 573. pp. 230-236. ISSN 0927-7757

https://doi.org/10.1016/j.colsurfa.2019.04.043

Resonance Properties of Quartz Crystal Microbalance Immersed in High Solid Content Suspensions

J.A. Botha[1], T.N. Hunter[1], D. Johannsmann[2], D. Austin[1], C.S. Hodges[1], G.A. Mackay[3], S.E. Woodbury[4], S. Biggs[5] and D. Harbottle[*1]

[1] School of Chemical and Process Engineering, University of Leeds, United Kingdom
[2] Institute of Physical Chemistry, Clausthal University of Technology, D-38678 Clausthal-Zellerfeld, Germany
[3] NNL Workington Laboratory, Cumbria, UK
[4] NNL Central Laboratory, Sellafield, Cumbria, UK
[5] The University of Western Australia, Australia

* D.H., E-mail: d.harbottle@leeds.ac.uk, T: +44(0) 113 343 4154

Abstract

The resonance properties, frequency and half-band-half-width, of a quartz crystal microbalance (QCM) immersed in concentrated suspensions of 16.2 vol% TiO_2 are shown to be a function of pH. The overall QCM response is dependent on the complex interactions between the QCM sensor and overlying particle suspension. Atomic force microscopy confirms pH dependent interaction forces between the QCM sensor (gold-coated) and a TiO_2 particle: a strong attraction is measured between pH 4 – 4.5, and the interaction becomes increasingly repulsive at all pH > 6.5. Yield stress measurements of the concentrated TiO_2 suspensions also confirm the changing particle-particle interaction strength as the pH is adjusted from acidic to basic conditions. For the chosen system, the total potential energy of interaction (V_T) between the sensor-suspension (Au-TiO_2) is comparatively stronger than the particle-particle (TiO_2-TiO_2) interaction; hence the QCM responds to changes in V_T sensor-suspension, as verified by the calculated interaction energy between two dissimilar surfaces (Hogg-Healy-Fuerstenau (HHF) theory), and not the suspension yield stress. Slight deviation between the measured QCM responses and the theoretical sphere-plate interaction strength is shown over a narrow pH range and likely corresponds to strengthening particle-particle interactions. Although the suspensions exhibit significant yield strengths, the QCM response can be suitably described by the sensor-suspension contact mechanics of inertial loading. Combined with our previous study[1], the current study confirms that the suspension yield strength can only be measured when V_T sensor-suspension is attractive and comparatively weaker than V_T particle-particle.

Introduction

The quartz crystal microbalance is a tool frequently used to study soft matter systems providing insight into deposited/adsorbed layer properties,[2] interactions between chemical and/or biological species, and the stability of deposited/adsorbed layers under different physicochemical conditions.[3-4] There is growing interest to study the influence of point contact loads (particles) on the QCM sensor resonance properties, with complexity now extending to probe the resonance properties in the presence of colloidal dispersions.

Until recently only a few researchers had considered the problem of particles (multiple particles) depositing onto an oscillating QCM sensor. With its nano-gram sensitivity, QCM is an ideal technique to study the tendency for particle-substrate interactions in changing chemical environments. Rafie Borujeny et al.[5] considered the effect of suspension pH on the interaction between silica (QCM sensor) and ceria nanoparticles. By varying the ceria slurry pH between 3 and 10, the authors observed high rates of particle deposition at pH 3 and pH 7, and much lower particle deposition rates (< 1 ng/cm^2.s) at pH 10. The authors explained the QCM response in terms of the total interaction energy as described by DLVO theory; for a particular ceria particle concentration, high deposition rates were shown to correspond to strong particle attraction to the silica QCM sensor.

Several authors use colloid theory to describe measured changes in the QCM resonance frequency as particles deposit onto the sensor. Gotoh et al.[6] used an extended-DLVO theory to include the potential energy of Lewis acid-base interactions, and correlated the primary minimum of the total potential energy to the number of particles deposited for a range of particle-substrate (sensor) interactions (Nylon 12 – polyethylene; polyethylene – Nylon 6; Nylon 12 – Nylon 6). Seo et al.[7] studied silica nanoparticles of varying size (~10 to 110 nm) interacting with silica QCM sensors. While the measured responses as a function of ionic strength were consistent with DLVO theory, the smallest silica particles exhibited the highest deposition (surface fractional coverage) which the authors attributed to a particle size-dependent hydration force. Inclusion of short-range repulsive hydration forces was also postulated by Dylla-Spears et al.[8] to explain negligible ΔF when DLVO theory predicts strong attraction between the silica particles and silica sensor (high ionic strength). Fatisson et al.[9] studied the initial deposition rates of colloidal TiO_2 particles (less than 100 nm) onto SiO_2 coated QCM-D sensors as a function of pH and ionic strength. At low ionic strength (< 5 mM $NaNO_3$), a clear dependency on pH was observed with the highest rate of particle deposition corresponding to the strongest attraction between the two surfaces (particle and sensor). At

high ionic strength (100 mM $NaNO_3$), the pH dependency diminished as the zeta potential of the TiO_2 particles approached 0 mV, with the measured QCM-D responses qualitatively described by the DLVO theory.

While QCM-particle deposition is now more commonly studied, deposition conditions often consider nanometer-sized particles at relatively low particle concentrations (monolayer and sub-monolayer coverage). At high particle concentrations and for large particles the resonance properties of the QCM sensor are sensitive to the contact mechanics between the particle and sensor. These effects have been highlighted by Zhuang et al.[10] who measured the QCM frequency response as particle-laden droplets evaporated on a gold-coated sensor. Negative frequency responses were measured when alumina particles were rigidly attached to the QCM sensor at sub-monolayer coverage, with behavior consistent to that previously discussed. At high particle concentration (> 1 wt%), particle multilayers were formed and the measured frequency shift was positive. The magnitude of the frequency shift was dependent on the particle size, with 1 µm alumina particles producing ΔF responses greater than 1000 Hz (3 – 5 wt% solids). Smaller positive frequency shifts were also measured for 50 nm alumina particles at high solid concentrations, with the effect attributed to the interaction between neighboring particles as well as the contact stiffness between the deposit mass and resonating sensor. Olsson et al.[11] measured positive frequency shifts across all overtones (n = 1 to 13) for 5 µm silica particles (depositing on a silica sensor) at sub-monolayer coverage, with changing ionic strength having a negligible effect on the QCM signal.

Positive frequency shifts resulting from particle-sensor contacts were first discussed by Dybwad[12], D'Amour et al.[13] and Pomorska et al.[14] who modelled the particle-QCM sensor interactions as a sphere-plate coupled resonance. Under conditions of small dissipative forces between the particle and the sensor, the coupled resonance model leads to

$$\frac{\Delta F + i\Delta\Gamma}{F_F} \approx \frac{-N_S m_S \omega}{\pi Z_q} \frac{1}{1-\frac{\omega^2}{\omega_S^2}} \qquad \text{Eq. 1}$$

where ΔF is the frequency shift, ΔΓ the half-band-half-width (HBHW) shift, F_F the fundamental mode resonance frequency of the sensor, N_S the number of particles, m_S the particle mass, Z_q the impedance of the AT-cut quartz sensor, ω the angular frequency of the sensor, and ω_S the angular frequency of the particle. The resonance frequency of the particle-sensor assembly is considered to be complex. We write $\omega_s^2 = \frac{\kappa_{eff}}{m_{eff}} + i\omega\frac{\xi_{eff}}{m_{eff}}$ with κ_{eff} a

spring constant, m_{eff} an effective mass and ξ_{eff} an effective friction coefficient. ξ_{eff} quantifies the dissipative components of the particle-sensor interaction and was not shown in Eq. 1 for simplicity. Two loading regimes may be considered within this model: i) inertial loading for $\omega << \omega_s$ and ii) elastic loading for $\omega >> \omega_s$. Under inertial loading Eq. 1 simplifies to

$$\frac{\Delta F + i\Delta\Gamma}{F_F} \approx \frac{-2FN_S m_S}{Z_q} \qquad \text{Eq. 2}$$

which is equivalent to the Sauerbrey equation[14-18] with $N_s m_s$ representing the mass per unit area and F the resonance frequency of the loaded sensor. Under these inertial loading conditions the resonance frequency decreases as mass deposits onto the sensor. Eq. 2 predicts $\Delta\Gamma \approx 0$, however $\Delta\Gamma$ is often found to be substantial. $\Delta\Gamma > 0$ may be rooted in either dissipative processes inside the adsorbate or in energy being dissipated into the medium beyond the adsorbate.

Under elastic loading conditions ($\omega \gg \omega_s$) Eq. 1 may be reduced to

$$\frac{\Delta F + i\Delta\Gamma}{F_F} \approx \frac{1}{\pi Z_q}\frac{N_S \kappa_S}{\omega} \qquad \text{Eq. 3}$$

where $\omega_S = \sqrt{\frac{\kappa_S}{m_S}}$ and κ_S is the stiffness of the sphere-plate contact. While this model is based on a single point contact, elastic loading and positive ΔF values have been reported for concentrated suspensions, where the particles seem to behave as a uniform adsorbed mass. This model is based on non-interacting point contacts. Elastic loading and positive ΔF values have been reported for concentrated particulate suspensions, where the contacts seem to be elastically independent in this sense.

For concentrated $Mg(OH)_2$ suspensions, our recent study showed the air-to-sample QCM resistance shift (a parameter directly proportional to the HBHW) increased with increasing yield stress.[1] The suspension yield stress was a function of the particle concentration with the pH and ionic strength kept constant. The QCM frequency response was found to be more complex and thought to be sensitive to the suspension properties (gel point and viscoelasticity), as well as the sensor-suspension loading mechanics (inertial and elastic loading). In the current study, we explore the QCM resonance properties when submerged in yield stress fluids of varying pH. Varying the pH of a 16.2 vol% TiO_2 suspension, relative contributions from TiO_2-

TiO_2 and TiO_2-gold (QCM sensor) interactions on the overall QCM resonance properties are elucidated, noting that the Hamaker constant TiO_2-H_2O-TiO_2 ($A_{131} = 0.00278 \times 10^{-20}$ J) [19-20] is two orders of magnitude smaller than TiO_2-H_2O-gold ($A_{132} = -0.253 \times 10^{-20}$ J).[21]

Materials and Methods

Hombitan S141 (supplied by Venator Ltd.) is an anatase grade of TiO_2 with a d_{50} of 0.62 µm. The particles were used as received. 100 mL batches of 16.2 vol% TiO_2 suspensions were prepared in 10^{-2} M NaCl (analytical grade, Fisher Scientific) using deionized water (Milli-Q grade) with a resistivity of 18.2 MΩ.cm. Suspensions were mixed using an overhead stirrer for 5 min to resemble a smooth paste and then pH adjusted using NaOH (ACS reagent, Sigma Aldrich) or HCl (AnalaR-grade, VWR International), mixed for a further 5 min and sealed before leaving overnight (min. 15 h) to equilibrate. Before each measurement the suspension pH was re-checked and adjusted if needed. All samples were pH adjusted from an initial pH 5.3 (natural condition).

Particle and substrate zeta potential: A Zetasizer Nano ZS (Malvern, UK) was used to measure the pH dependent particle zeta potential via the Henry approximation.[22] Dilute suspensions (0.25 vol%) of TiO_2 were prepared in 10^{-2} M NaCl and left to equilibrate. The pH was adjusted from the natural pH to either acidic or basic conditions using HCl or NaOH before sonicating the suspension for 5 min and then pipetting a few mL into a zeta cell. An average of 10 measurements at each pH is reported with error bars showing the variance. A SurPASS Electrokinetic Analyser (Anton Paar, USA) was used to measure the streaming potential of a 5 MHz AT-cut gold-coated 25.4 mm diameter QCM sensor (Stanford Research Systems) that was cut to size (d = 14 mm) by laser ablation. The sensor was cleaned in 2 vol% Decon-90 (Decon™ D901, Fisher Scientific) solution (diluted using Milli-Q grade water), sonicated for 10 min and rinsed thoroughly with deionized water, before being dried using N_2 gas. Background electrolyte of 10^{-2} M NaCl was used and the pH adjusted between pH 3.5 – 9.5. Two gold-coated sensors were clamped parallel to each other in the flow cell sample holder and perpendicular to the direction of flow. The background electrolyte solution of desired pH was then pumped through the flow cell to induce ion mobility of the outer Helmholtz plane in the direction of flow, leading to charge accumulation at one end of the flow cell. The potential difference leads to a reversal in the flow of charge to maintain charge equilibrium. Electrodes at each end of the flow cell measure the potential difference (streaming potential, ΔV) which

is dependent on the pressure drop (ΔP) in the flow cell. The pressure drop-dependent streaming potential was used to calculate the zeta potential by the Helmholtz-Smoluchowski approach.[23]

X-ray Diffraction (XRD): Dry TiO_2 powder was mounted into a D8 XRD (Bruker, US) with Cu-Kα radiation (λ = 0.15418 nm) in the 2θ range of 20º - 80º and step size of 0.016˚. Lattice parameters were obtained from the International Centre for Diffraction Data – Powder Diffraction File database (ICDD-PDF4+).

Atomic force microscopy (AFM): The pH-dependent interaction forces between a single TiO_2 sphere (Sachtopore NP, Sachtleben Chemie) and gold-coated QCM sensor was measured by AFM. To prepare the colloidal probe, a tipless silicon-coated cantilever (Nanosensors, USA. Supplied by NanoAndMore, Germany) with a spring constant of 0.2 N/m was gently dipped into a thin line of Araldite rapid epoxy resin (Huntsman Advanced Materials) to wet the cantilever with a small drop of the epoxy resin. The cantilever was then immediately withdrawn and positioned over the centre of a 20 µm sphere and lowered into contact with the single particle. The cantilever-particle couplet were held in contact for 10 min to ensure the epoxy resin had partially set before retracting the colloidal probe from the substrate. The colloidal probe was left overnight to allow the epoxy glue to cure fully in the BioScope II AFM cantilever holder (Veeco, USA). Before measurement, the colloidal probe was washed by submerging in deionised water followed by the background electrolyte solution and calibrated using the X-Y calibration function in the NanoScope V710 software.

The gold-coated QCM sensor was mounted on a glass slide using the same epoxy resin and left overnight for the epoxy resin to set. The sensor was washed in 2 vol% Decon-90 solution for 5 min, rinsed thoroughly with deionised water and dried with N_2 gas. The sensor was mounted on the AFM stage and submerged in 10^{-2} M NaCl of adjusted pH. The measured deflection of the AFM cantilever is proportional to the force acting on the colloidal particle and can be obtained by multiplying the spring constant (0.2 N/m) by the deflected distance. The colloidal probe approach and retract speed was kept constant at 150 nm/s and multiple force curves (> 10) were collected at several different locations on the gold-coated sensor to achieve a reasonable statistical average from each location on the sample.

Yield stress: The pH-dependent yield stress of 16.2 vol% TiO_2 suspensions were measured using a viscometer (Brookfield DV-II+ Pro Viscometer, UK) with a 4-blade vane of dimensions: H = 43.33 mm and D = 21.67 mm. A detailed explanation of the measurement setup has been provided in our earlier publication.[1] Briefly, the vane was lowered below the

suspension interface to a constant height identified by a 'notch' on the geometry. With the vane fully submerged, the vane was rotated at 1 rpm for 2 min with the viscometer torque continuously measured. The suspension yield stress was then determined from the maximum torque measured. Wall effects were minimized with a vane-to-cylinder ratio of 1:3.5 and the sample beaker was clamped to avoid sample rotation during the measurement.

Quartz crystal microbalance (QCM): An impedance monitoring QCM (provided by Clausthal University of Technology, Germany) operating in 'reflection mode' with a dip probe attached (Stanford Research Systems, USA) was used to measure the sensor resonance frequency and HBHW shifts. The dip probe housed a 25.4 mm, 5 MHz AT-cut gold-coated sensor that was cleaned following the method previously described (see AFM section). The cleaned QCM sensor was calibrated in air by locating and fitting the peaks obtained when the electrical admittance of the resonator as a function of oscillation frequency is mapped.[24] The resonance properties of overtones 1, 3, 5, 7, 9, 11 (equivalent to frequencies of 5, 15, 25, 35, 45, and 55 MHz) were recorded until a stable baseline had been established (~30 min). The QCM dip probe was then submerged into the 16.2 vol% TiO_2 suspension of known pH and rotated several times. With the sensor fully submerged, the QCM was re-calibrated by refitting the electrical admittance peaks. The resonance frequency and HBHW were measured until a new baseline was established (measured for ~ 45 min such that the drift in resonance frequency was < 0.1 Hz/min). The air-to-sample resonance frequency (ΔF) and HBHW ($\Delta \Gamma$) were determined from the shift in steady-state signals.

Results and Discussion

Particle and QCM sensor characterization: Background subtracted XRD analysis of the dried Hombitan powder (Fig. 1) revealed the sample to be composed predominantly of a crystalline TiO_2 phase identified as Anatase (ICDD: 01-075-2546). Comparing the peak positions with an anatase reference from the American Mineralogist Crystal Structure Database Record (RRUFF: R060277.9) showed some peak broadening, possibly resulting from the presence of small crystallite sizes and/or amorphous material within the sample matrix.[25] SEM images (Hitachi SU8230 SEM), see inset Fig. 1, show small crystallites typically ranging from ~50 to 80 nm having un-defined edges which suggests the presence of amorphous material.

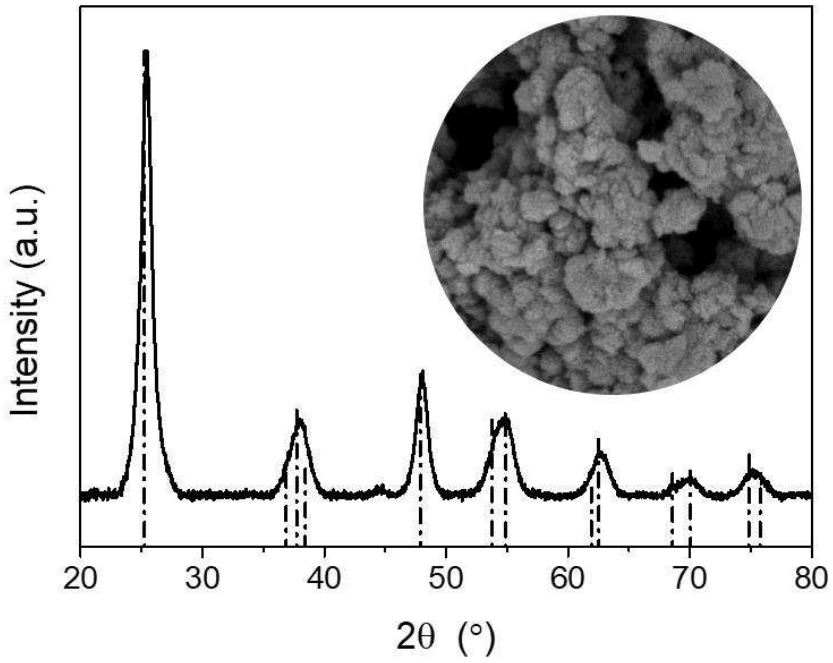

Figure 1. Hombitan S141 (TiO_2) powder XRD spectra (solid lines) and SEM image with the inset diameter = 1 µm. The dashed-dot lines represent the reference peaks for pure anatase, taken from the American Mineralogist Crystal Structure Database Record (RRUFF: R060277.9).

The zeta potential of hydrated TiO_2 (Fig. 2) showed a pH dependence typical of anatase TiO_2 [26] with an iso-electric point (i.e.p.) of pH 6.6. Moreover, the zeta potential of the gold-coated QCM sensor (determined from streaming potential measurement) was negative over the pH range 3.5-9.1, hence the sensor i.e.p. is below pH 3.5. These values are in reasonable agreement with published data[27-28] and confirmed that the deposited gold layer on the QCM sensor was suitably thick to screen any contribution from the underlying chrome layer.

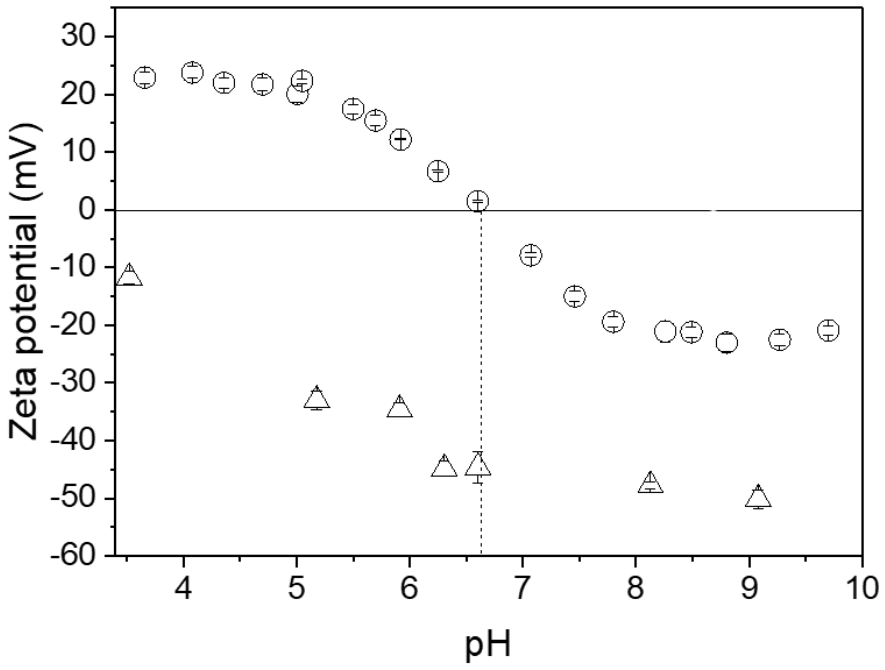

Figure 2. Zeta potentials of TiO_2 (open circles) and gold-coated QCM sensor (open triangles) as a function of pH in 10^{-2} M NaCl background electrolyte. The dashed line represents the i.e.p. of TiO_2 (pH 6.6).

Particle-QCM sensor and particle-particle interactions: The interaction forces between the gold-coated QCM sensor and a spherical TiO_2 particle (analogue for Hombitan S141 TiO_2) was measured by AFM, see Fig. 3. At pH 4.0, the TiO_2 particle is positively charged and the TiO_2 colloid probe experiences an attraction at separations less than ~15 nm from the gold-coated sensor (Fig. 3a). When the pH was adjusted to pH 8.3, a long-range repulsive force was measured. Since the zeta potential of the gold-coated sensor was negative across the pH range, the measured change from attraction to repulsion by AFM is consistent with the TiO_2 zeta potential curve shown in Fig. 2.

The maximum attractive force F/R (nN/μm), taken to be the most negative force measured on approach, is shown in Fig. 3b as a function of pH. Experimental variability depends on the magnitude of the overall attraction and is possibly affected by local surface variance due to sorbed oxide, hydroxide and chloride species.[27, 29] A pH dependence is observed with the strongest attraction measured in the pH range 4 to 4.5. As the pH is increased the measured attraction weakens, becoming negligible (i.e. repulsive interaction) when the pH $\geq$ 6.6, albeit there is observed jump-to-contact at very short range, indicative of the van der Waals

component becoming dominant. The pH dependent AFM data confirms that the single TiO_2 sphere is a good analogue for Hombitan S141 particles showing a similar pH dependence.

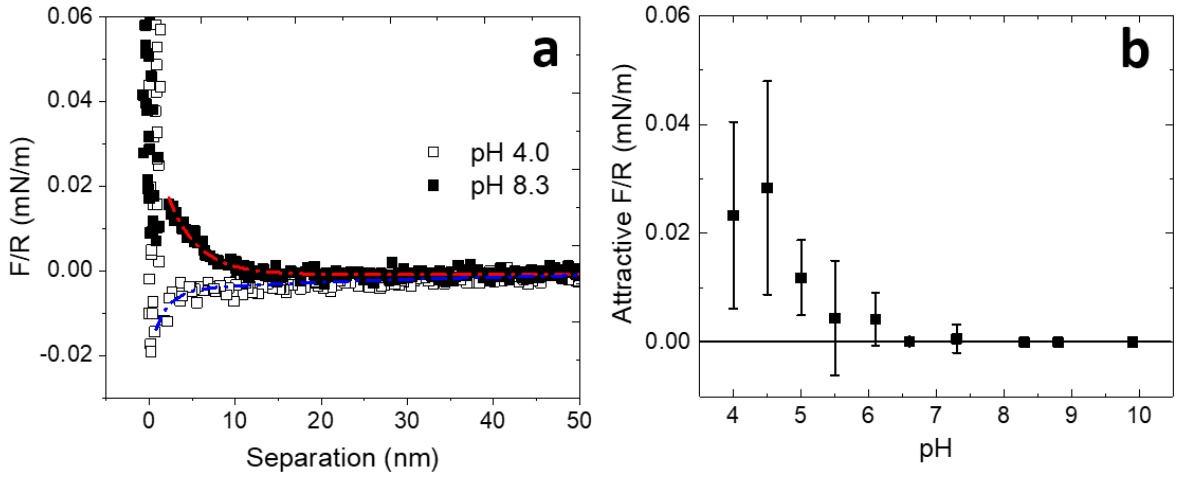

Figure 3. a) Typical AFM interaction forces between an approaching TiO_2 particle (particle radius 10 µm) and a gold-coated QCM sensor in 10^{-2} M NaCl at pH 4.0 and 8.3 (n.b. to improve the clarity of the data presented, 4 out of 5 data points have been omitted from the original data set and lines to guide the eye included). b) Average values for the strongest attraction measured on approach in 10^{-2} M NaCl and at different pH values. Only values when F/R < 0 mN/m were counted in the averaging. Error bars represent 1 standard deviation.

With the particle zeta potential varying with pH, the particle-particle interaction strength can vary substantially and thus modify the rheology of the concentrated particle suspension. Fig. 4 shows the yield stress of a 16.2 vol% TiO_2 suspension as a function of pH between pH 4.3 and 9.4. At low pH (pH 4.3) the suspension appeared 'milky' with no measurable yield stress. As the pH was increased and the particle zeta potential approached the i.e.p., the suspension yield stress increased markedly. This behaviour is a direct consequence of increased attraction (weakening electrostatic repulsive force) between neighbouring particles, allowing them to form aggregates and larger clusters which eventually network to induce a finite yield stress in the suspension.[30-32] The maximum yield stress was measured at pH 5.9, slightly below the measured i.e.p. While this difference is not entirely understood, a similar behaviour has been reported previously for anatase suspensions and attributed to the rheology and electrokinetic techniques responding to electric potentials at two different distances from the surface.[33] Beyond pH 5.9 the suspension yield stress decreased linearly with increasing pH, corresponding to the increased negative zeta potential of the TiO_2 particles.

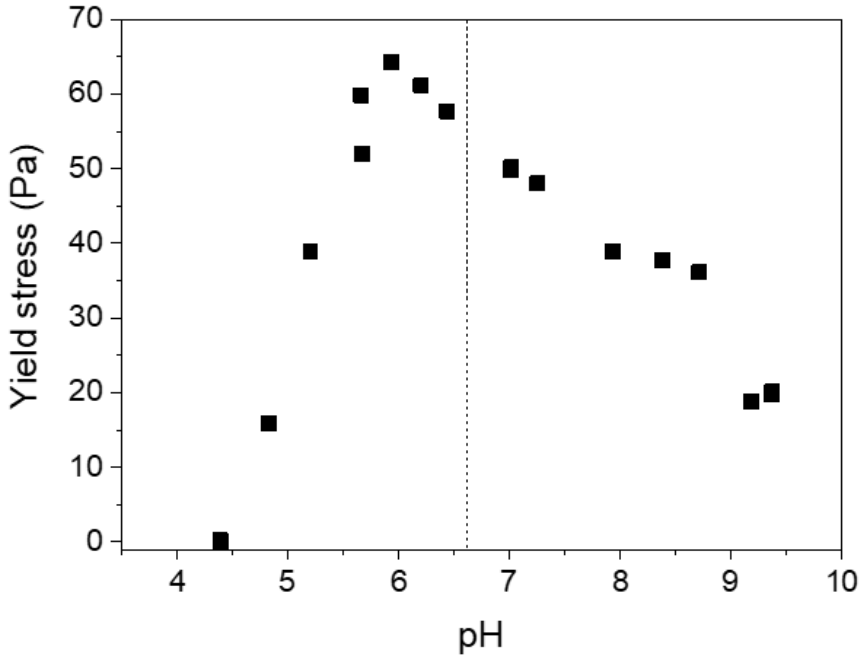

Figure 4. pH dependent yield stress of 16.2 vol% TiO_2 suspensions in 10^{-2} M NaCl. The dashed line corresponds to the i.e.p. of TiO_2 (pH 6.6).

The Hogg-Healy-Fuerstenau (HHF)[34] equation was solved using the measured zeta potential values (Fig. 2) to calculate the total potential energy of interaction (V_T) between Au-TiO_2 (sensor-particle) and compared to V_T for TiO_2-TiO_2 (particle-particle) as determined for two similar spheres interacting. The HHF theory describes the potential energy of interaction (contributions from van der Waals forces and the electrostatic repulsive force) between two dissimilar surfaces. The attractive (V_A) and repulsive (V_R) forces between a sphere and flat plate are given by Eqs. 4 and 5, with the total potential energy of interaction given by $V_T = V_A + V_R$ [35-36]:

$$V_R = 2\pi\varepsilon_r\varepsilon_0 a_p \zeta_p \zeta_c \left\{\ln\left[\frac{1+e^{-\kappa a_p H}}{1-e^{-\kappa a_p H}}\right] + \frac{(\zeta_p^2+\zeta_c^2)}{2\zeta_p\zeta_c}\ln[1-e^{-2\kappa a_p H}]\right\} \quad \text{Eq. 4}$$

$$V_A = -\frac{A_{132} a_p}{6H} \quad \text{Eq. 5}$$

where ε_r is the permittivity of the medium, ε_0 the permittivity of free space, a the radius, ζ the zeta potential, κ the inverse Debye length, where $\kappa^{-1} = \frac{0.304\times10^{-9}}{\sqrt{M}}$ at 25℃, M the molar concentration of electrolyte in solution, H the separation distance and A_{132} the TiO_2-water-Au

Hamaker constant (= -0.2534×10^{-20} J). [19-20] Subscripts p and c denote the particle and the QCM sensor, respectively.

Fig. 5 shows the total potential energy of interaction (V_T) at a separation distance of 5 nm (distance arbitrarily taken for relative comparison) between the similar (particle-particle) and dissimilar (sensor-particle) surfaces. To compare both interactions at equivalent pH values (pH range ~3.6 to 9.8), a Boltzmann fit (R^2 0.9774) of the gold-coated sensor zeta potentials was made. To calculate the electrostatic repulsive force the particle radius was taken to be 0.31 µm, representing the modal particle size as measured by the Zetasizer Nano ZS (Fig. S1). The magnitude of the sensor-particle interaction strength is greater than the particle-particle interaction strength in both acidic and basic conditions, partially influenced by the differing Hamaker constants; TiO_2-H_2O-TiO_2 (A_{131} = 0.00278×10^{-20} J) being two orders of magnitude smaller than TiO_2-H_2O-gold (A_{132} = -0.253×10^{-20} J). At low pH, the sensor-particle interaction is strongly attractive while the TiO_2 particles remain dispersed. At high pH, both interactions are repulsive when all surfaces are negatively charged. For TiO_2-TiO_2 the pH at maximum attraction corresponds to the particle i.e.p. and for TiO_2-Au this condition is found at a lower pH and corresponds to the largest potential difference between the two surfaces. Such behaviour is complementary to the AFM force measurements (Fig. 3b) which showed the strongest attraction between the TiO_2 particle and gold-coated QCM sensor to be pH 4.5.

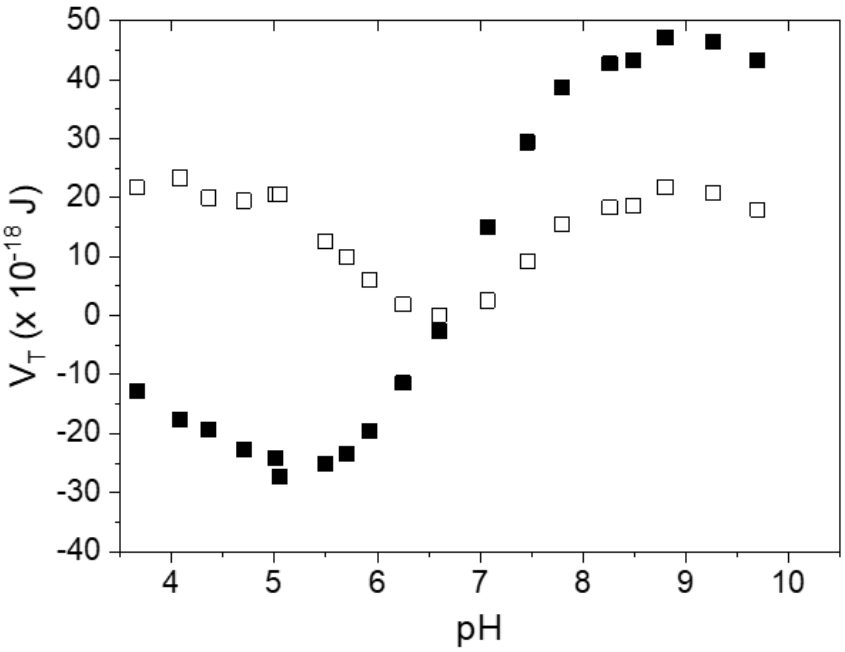

Figure 5. The calculated total potential energy of interaction (V_T) at a separation distance of 5 nm between TiO_2-Au (closed symbols) and TiO_2-TiO_2 (open symbols). The electrostatic repulsive force was calculated using values: $\varepsilon_r = 80.3$ J/V^2; $\varepsilon_0 = 8.854 \times 10^{-12}$ J/V^2; $a_p =$ 0.31 μm; ζ_p taken from Fig. 2; ζ_c determined from the Boltzmann fit of the data in Fig. 2; and $M = 10^{-2}$ M NaCl.

QCM measurements: Our previous research considered $Mg(OH)_2$ suspensions and confirmed the sensitivity of the QCM to detect changes in suspension yield stress (varied by changing the solids concentration).[1] The suspension pH was kept constant and close to the i.e.p. of $Mg(OH)_2$ (zeta potential of -7 ± 4 mV at pH 10.2). Using the sphere-plate HHF theory, the total potential energy of interaction between $Mg(OH)_2$ and the gold-coated QCM sensor in water is approximately -16×10^{-18} J (using the Hamaker constant for MgO = 12.1×10^{-20} J), confirming strong attraction between the QCM sensor and overlying suspension. In the current study, changing pH altered both the suspension yield stress and the interaction strength between the gold-coated QCM sensor and TiO_2 particles (Figs. 3 and 4). The influence of changing two parameters simultaneously, i.e. the suspension yield stress and the QCM sensor-particle suspension interaction strength, on the response of the QCM has not yet been considered.

The $-\Delta F/n$ and $\Delta\Gamma/n$ responses of the QCM when submerged in 16.2 vol% TiO_2 suspensions of varying pH are shown in Fig. 6a (inset $\Delta\Gamma/n$). The sensor overtones (n = 3 to 11) all show

the same general trend with pH. The frequency initially increases (from low pH) to a maximum $-\Delta F/n$ at pH 4.5 followed by a decrease, reaching a constant value at higher pH values (pH > 7). Most of the $\Delta\Gamma/n$ responses also show an increase, to pH 5, followed by a gradual decrease at higher pH values. The exception is the n = 1 $\Delta\Gamma$ data set (data not shown), where the response was found to generally decrease across the pH range investigated. (The fundamental (n = 1) often behaves differently from the other modes because the flexural admixtures to shear vibration pattern are strong. These launch compressional waves into the sample, which causes artifacts). The pH responses of $-\Delta F/n$ and $\Delta\Gamma/n$ do not directly correspond with the suspension yield stress data (Fig. 4). Both $-\Delta F/n$ and $\Delta\Gamma/n$ increase as the suspension yield stress increases (low pH), consistent with our previous study,[1] although the measured QCM responses begin to decrease before the maximum yield stress (Fig. 4) is reached (pH 5.9). At higher pH values the $-\Delta F/n$ and $\Delta\Gamma/n$ responses become independent of the suspension pH, while the suspension yield stress shows an approximately 30 Pa decrease (~50% of peak) over the same pH range. The observed difference in trends between the QCM responses and suspension yield stress suggests that the QCM resonance properties are not only influenced by the suspension yield stress.

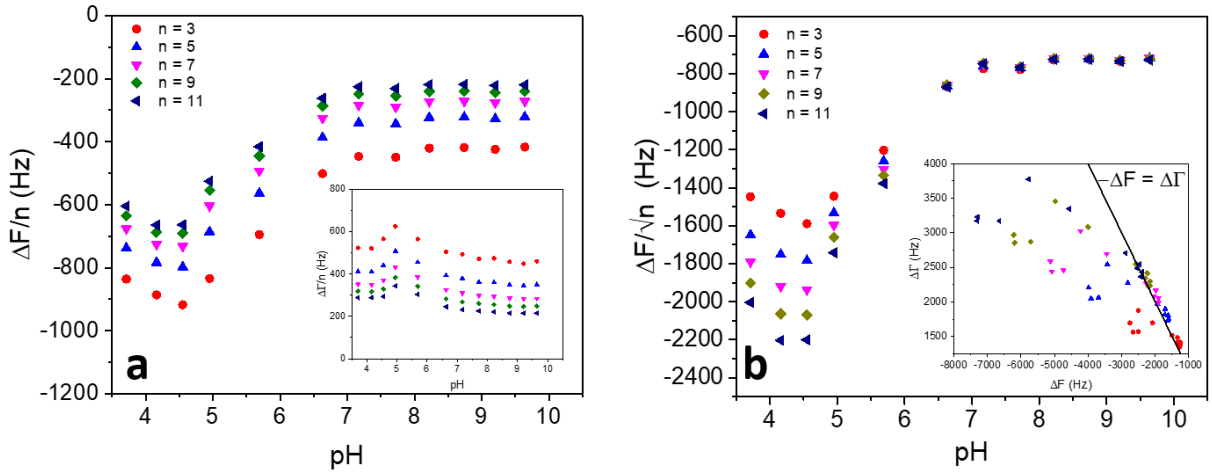

Figure 6. QCM resonance properties a) $\Delta F/n$ (inset: $\Delta\Gamma/n$) as the QCM is submerged (air-to-sample shifts) into 16.2 vol% TiO_2 suspension of desired pH and 10^{-2} M NaCl background electrolyte. b) pH dependent ΔF normalized by $\sqrt{n}$. Inset: ΔF versus $\Delta\Gamma$ for all overtones with the condition $-\Delta F = \Delta\Gamma$ shown by the solid line. The condition $-\Delta F \neq \Delta\Gamma$ is at pH $\leq$ 6.6 and is true for all measured overtones.

Plotting $\Delta F/\sqrt{n}$, as is typical for the scaling of Newtonian liquids, reveals more about the signal response in acidic and basic conditions. At pH > 7, $\Delta F/\sqrt{n}$ tends towards the Gordon-

Kanazawa-Mason limit for an air-to-water transition, $\Delta F/\sqrt{n} = -721$ Hz for n = 3 at pH 9.6, with variation of ± 5 Hz across the overtones 5, 7, 9 and 11 (for water $\Delta F/\sqrt{n} = -714$ Hz), where the resonance frequency is proportional to the square root of the liquid density-viscosity product[37-39]. Although the QCM is submerged in a yield stress suspension (Fig. 4), the measured $\Delta F/\sqrt{n}$ suggests that the QCM responds to the liquid-loading (water) and does not detect the particles. This is confirmed in Fig. 6b inset where the overtone responses for pH > 6.6 correspond to $-\Delta F/\Delta\Gamma = 1$, as expected for a Newtonian liquid (for a Newtonian liquid, the shear stress, σ, is related to the tangential velocity, u, as $\sigma = Z_{liq}u = (i\omega\rho\eta)^{1/2}u$. The complex frequency shift $\Delta F + i\Delta\Gamma$ is proportional to the shear stress at the resonator surface.[16] Given that $i^{1/2} = (1+i)/2^{1/2}$, ΔF and $\Delta\Gamma$ take the same numerical values (signs disregarded in this argument)). Eventually there is an overtone dependent limit when the ratio no longer holds and this represents the changing interaction strength between the QCM sensor and suspension particles. Below pH 6 the overtone responses ($\Delta F/\sqrt{n}$) diverge (Fig. 6b) with the largest measured deviation between overtones 3 and 11 found at pH 4.2. Below pH 6.6, Fig. 5 confirms attraction between the QCM sensor and the overlying particle suspension and hence, the QCM response likely becomes a complex function of: i) fluid properties (density and viscosity), ii) particle properties (density, hardness),[14] iii) particle-sensor contact (number of contacts, strength of contact and contact mechanics),[40] and iv) particle-particle interactions (number of contacts and strength of contact).[8] While it is difficult to differentiate between each contributing factor in this complex system, Fig. 7 compares the $\Delta F/n$ and $1/\Delta\Gamma/n$ responses for the 3rd overtone to the calculated V_T for a sphere-plate interaction (Fig. 5). The generalization that the QCM response correlates to V_T for sphere-plate interaction is likely an oversimplification, and comparison of the two data sets is not exact across the pH range 5.5 – 7.5, i.e. in the region where the TiO_2-TiO_2 attraction becomes more significant (Fig. 5), possibly demonstrating some influence of the underlying suspension yield stress. However, based on the understanding of point contact loads, Fig. 7 does confirm that the response of the QCM remains in the inertially-dominant loading regime, hence ΔF remains a parameter that is proportional to the apparent mass per unit area (Eq. 2), in this study ΔF is strongly influenced by the total potential of energy of interaction between the QCM sensor and suspension particles.

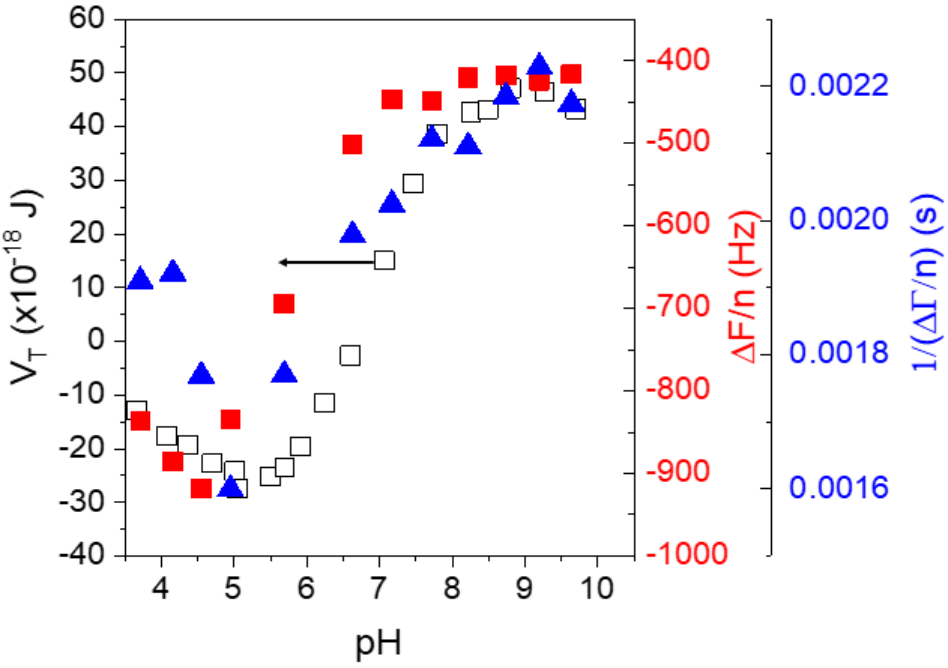

Figure 7. V_T (open squares) for sphere-plate interactions (Eqs. 4 and 5) compared to ΔF/n (closed squares) and 1/(ΔΓ/n) (closed triangles) where n is the 3rd overtone. Test sample: 16.2 vol% TiO_2 in 10^{-2} M NaCl.

Conclusions

The current study considered the frequency and HBHW responses by immersing a QCM in high solids content yield stress suspensions. The suspension yield stress increased from 0 Pa to 64 Pa when the pH was increased from 4.4 to 5.9 before decreasing slightly as the pH was increased to 9.4. Over the same pH range both −ΔF/n and ΔΓ/n responses fluctuated and were shown to be independent of the yield stress when the pH > 7, corresponding to a strong repulsion in the sensor-particle interaction. At high pH, ΔF/√n responses approximated to the liquid loading limit described by the Gordon-Kanazawa-Mason theory, confirming an insensitivity of the QCM responses to the suspension particles. At lower pH values, opposing zeta potential values of the QCM sensor and TiO_2 particles led to strong attraction between the two surfaces. In general, the QCM responses (ΔF/n, 1/(ΔΓ/n)) were shown to be in reasonable agreement with the theoretically calculated sphere-plate total interaction energy. Slight deviation may have resulted from the oversimplification of treating a complex system by a single parameter. Consideration of other parameters such as the particle-particle interaction strength may lead to a more comprehensive understanding of the overall QCM responses, although as yet this has not been quantified. Finally, immersing the QCM in yield stress

suspensions, this study has shown that the QCM resonance remains in the inertial loading regime and does not transition to elastic loading, with the sensor-particle interaction strength modulating the “apparent mass” detected by the QCM.

Acknowledgements

The authors acknowledge the Engineering and Physical Sciences Research Council (EPSRC), the National Nuclear Laboratory (NNL) and Sellafield Ltd. for providing financial support (EPSRC iCASE 13220135). The authors are also very grateful to Jie Ru from the Department of Chemical and Materials Engineering, University of Alberta who completed the streaming potential measurements.

References

1. Botha, J. A.; Ding, W.; Hunter, T. N.; Biggs, S.; Mackay, G. A.; Cowley, R.; Woodbury, S. E.; Harbottle, D., Quartz crystal microbalance as a device to measure the yield stress of colloidal suspensions. Colloids and Surfaces A: Physicochemical and Engineering Aspects **2018,** 546, 179-185.
2. Yu, K.; Hodges, C.; Biggs, S.; Cayre, O. J.; Harbottle, D., Polymer Molecular Weight Dependence on Lubricating Particle–Particle Interactions. Industrial & Engineering Chemistry Research **2018,** 57 (6), 2131-2138.
3. Zhang, H.; Tangparitkul, S.; Hendry, B.; Harper, J.; Kim, Y. K.; Hunter, T. N.; Lee, J. W.; Harbottle, D., Selective separation of cesium contaminated clays from pristine clays by flotation. Chemical Engineering Journal **2019,** 355, 797-804.
4. Tamiz Bakhtiari, M.; Harbottle, D.; Curran, M.; Ng, S.; Spence, J.; Siy, R.; Liu, Q.; Masliyah, J.; Xu, Z., Role of caustic addition in bitumen–clay interactions. Energy & Fuels **2015,** 29 (1), 58-69.
5. Rafie Borujeny, E.; Miao, M.; Pirayesh, H.; Xu, Z.; Cadien, K., An investigation of the deposition of ceria on silica by quartz crystal microbalance: Observations on the effect of many body interactions. Colloids and Surfaces A: Physicochemical and Engineering Aspects **2017,** 522, 207-217.
6. Gotoh, K.; Nakata, Y.; Tagawa, M., Evaluation of particle deposition in aqueous solutions by the quartz crystal microbalance method. Colloids and Surfaces A: Physicochemical and Engineering Aspects **2006,** 272 (1-2), 117-123.
7. Seo, J.; Kim, J. H.; Lee, M.; Moon, J.; Yi, D. K.; Paik, U., Size-dependent interactions of silica nanoparticles with a flat silica surface. J Colloid Interf Sci **2016,** 483, 177-184.
8. Dylla-Spears, R.; Wong, L.; Shen, N.; Steele, W.; Menapace, J.; Miller, P.; Feit, M.; Suratwala, T., Adsorption of silica colloids onto like-charged silica surfaces of different roughness. Colloids and Surfaces A: Physicochemical and Engineering Aspects **2017,** 520, 85-96.
9. Fatisson, J.; Domingos, R. F.; Wilkinson, K. J.; Tufenkji, N., Deposition of TiO2 Nanoparticles onto Silica Measured Using a Quartz Crystal Microbalance with Dissipation Monitoring. Langmuir **2009,** 25 (11), 6062-6069.
10. Zhuang, H.; Lu, P.; Lim, S. P.; Lee, H. P., Study of the evaporation of colloidal suspension droplets with the quartz crystal microbalance. Langmuir **2008,** 24 (15), 8373-8378.
11. Olsson, A. L. J.; van der Mei, H. C.; Johannsmann, D.; Busscher, H. J.; Sharma, P. K., Probing Colloid–Substratum Contact Stiffness by Acoustic Sensing in a Liquid Phase. Anal Chem **2012,** 84 (10), 4504-4512.
12. Dybwad, G., A sensitive new method for the determination of adhesive bonding between a particle and a substrate. Journal of applied physics **1985,** 58 (7), 2789-2790.
13. D'Amour, J. N.; Stalgren, J. J. R.; Kanazawa, K. K.; Frank, C. W.; Rodahl, M.; Johannsmann, D., Capillary aging of the contacts between glass spheres and a quartz resonator surface. Phys Rev Lett **2006,** 96 (5).
14. Pomorska, A.; Shchukin, D.; Hammond, R.; Cooper, M. A.; Grundmeier, G.; Johannsmann, D., Positive Frequency Shifts Observed Upon Adsorbing Micron-Sized Solid Objects to a Quartz Crystal Microbalance from the Liquid Phase. Anal Chem **2010,** 82 (6), 2237-2242.
15. Sauerbrey, G., Verwendung Von Schwingquarzen Zur Wagung Dunner Schichten Und Zur Mikrowagung. Z Phys **1959,** 155 (2), 206-222.
16. Johannsmann, D., Viscoelastic, mechanical, and dielectric measurements on complex samples with the quartz crystal microbalance. Phys Chem Chem Phys **2008,** 10 (31), 4516-4534.

17. D'amour, J.; Stålgren, J. R.; Kanazawa, K.; Frank, C.; Rodahl, M.; Johannsmann, D., Capillary aging of the contacts between glass spheres and a quartz resonator surface. Phys Rev Lett **2006,** 96 (5), 058301.
18. Vittorias, E.; Kappl, M.; Butt, H.-J.; Johannsmann, D., Studying mechanical microcontacts of fine particles with the quartz crystal microbalance. Powder technology **2010,** 203 (3), 489-502.
19. Gómez-Merino, A.; Rubio-Hernández, F.; Velázquez-Navarro, J.; Galindo-Rosales, F.; Fortes-Quesada, P., The Hamaker constant of anatase aqueous suspensions. J Colloid Interf Sci **2007,** 316 (2), 451-456.
20. Gregory, J., Particles in water: properties and processes. CRC Press: 2005.
21. Ederth, T., Computation of Lifshitz−van der Waals Forces between Alkylthiol Monolayers on Gold Films. Langmuir **2001,** 17 (11), 3329-3340.
22. Henry, D. C.; Lapworth, A., The cataphoresis of suspended particles. Part I.—The equation of cataphoresis. Proceedings of the Royal Society of London. Series A, Containing Papers of a Mathematical and Physical Character **1931,** 133 (821), 106-129.
23. Shapiro, A.; Renaud, P.; Probstein, R. F., Preliminary studies on the removal of chemical-species from saturated porous-media by electroosmosis. Physicochemical Hydrodynamics **1989,** 11 (5-6), 785-802.
24. Johannsmann, D., The Quartz Crystal Microbalance in Soft Matter Research. Springer: 2014.
25. Bates, S.; Zografi, G.; Engers, D.; Morris, K.; Crowley, K.; Newman, A., Analysis of amorphous and nanocrystalline solids from their X-ray diffraction patterns. Pharmaceutical research **2006,** 23 (10), 2333-2349.
26. Lakshminarasimhan, N.; Bae, E.; Choi, W., Enhanced Photocatalytic Production of H2 on Mesoporous TiO2 Prepared by Template-Free Method: Role of Interparticle Charge Transfer. The Journal of Physical Chemistry C **2007,** 111 (42), 15244-15250.
27. Giesbers, M.; Kleijn, J. M.; Stuart, M. A. C., The electrical double layer on gold probed by electrokinetic and surface force measurements. J Colloid Interf Sci **2002,** 248 (1), 88-95.
28. Sylvestre, J. P.; Poulin, S.; Kabashin, A. V.; Sacher, E.; Meunier, M.; Luong, J. H. T., Surface chemistry of gold nanoparticles produced by laser ablation in aqueous media. J Phys Chem B **2004,** 108 (43), 16864-16869.
29. Barten, D.; Kleijn, J.; Duval, J.; Leeuwen, H. v.; Lyklema, J.; Cohen Stuart, M., Double layer of a gold electrode probed by AFM force measurements. Langmuir **2003,** 19 (4), 1133-1139.
30. Leong, Y.-K.; Boger, D. V.; Scales, P. J.; Healy, T. W.; Buscall, R., Control of the rheology of concentrated aqueous colloidal systems by steric and hydrophobic forces. Journal of the Chemical Society, Chemical Communications **1993,** (7), 639-641.
31. Leong, Y. K.; Scales, P. J.; Healy, T. W.; Boger, D. V., Effect of particle size on colloidal zirconia rheology at the isoelectric point. Journal of the American Ceramic Society **1995,** 78 (8), 2209-2212.
32. KwongáLeong, Y., Rheological evidence of adsorbate-mediated short-range steric forces in concentrated dispersions. Journal of the Chemical Society, Faraday Transactions **1993,** 89 (14), 2473-2478.
33. Kosmulski, M.; Gustafsson, J.; Rosenholm, J. B., Correlation between the zeta potential and rheological properties of anatase dispersions. J Colloid Interf Sci **1999,** 209 (1), 200-206.
34. Hogg, R.; Healy, T. W.; Fuerstenau, D. W., Mutual coagulation of colloidal dispersions. Transactions of the Faraday Society **1966,** 62 (0), 1638-1651.
35. Israelachvili, J. N., Intermolecular and surface forces. Academic press: 2011.
36. Gu, Y., The electrical double-layer interaction between a spherical particle and a cylinder. J Colloid Interf Sci **2000,** 231 (1), 199-203.

37. Martin, S. J.; Frye, G. C.; Ricco, A. J.; Senturia, S. D., Effect of surface roughness on the response of thickness-shear mode resonators in liquids. Anal Chem **1993,** 65 (20), 2910-2922.
38. Mason, W. P.; Baerwald, H., Piezoelectric crystals and their applications to ultrasonics. Physics Today **1951,** 4, 23.
39. Kanazawa, K. K.; Gordon, J. G., The Oscillation Frequency of a Quartz Resonator in Contact with a Liquid. Anal Chim Acta **1985,** 175 (Sep), 99-105.
40. Astrid, P.; Arne, L.; Diethelm, J., Coupled resonances allow studying the aging of adhesive contacts between a QCM surface and single, micrometer-sized particles. Nanotechnology **2015,** 26 (48), 484001.